Precision Engineering xxx (2016) xxx–xxx

Contents lists available at ScienceDirect

Precision Engineering

journal homepage: www.elsevier.com/locate/precision

A coupled dynamics, multiple degree of freedom process damping model, Part 1: Turning

Christopher T. Tyler, John R. Troutman, Tony L. Schmitz*

University of North Carolina at Charlotte, Charlotte, NC, United States

ARTICLE INFO

Article history:
Received 1 May 2015
Received in revised form 10 February 2016
Accepted 21 March 2016
Available online xxx

Keywords:
Machining
Chatter
Stability
Process damping
Simulation

ABSTRACT

Self-excited vibration, or chatter, is an important consideration in machining operations due to its direct influence on part quality, tool life, and machining cost. At low machining speeds, a phenomenon referred to as process damping enables stable cutting at higher depths of cut than predicted with traditional analytical models. This paper describes an analytical stability model which includes a process damping force that is dependent on the surface normal velocity, chip width, cutting speed, and an empirical process damping coefficient. Model validation is completed using time domain simulation and turning experiments. The results indicate that the multiple degree of freedom model is able to predict the stability boundary using a single process damping coefficient.

1. Introduction

Process damping is a phenomenon that enables increased depths at cut at low cutting speeds in machining operations. When its effect is added to the analytical stability lobe diagram, a valuable predictive capability is afforded to process planners for a priori selection of machining parameters. It enables process planners to select stable {spindle speed, depth of cut} combinations for both:

- hard-to-machine materials, that are restricted to low cutting speeds due to prohibitive tool wear, and, therefore, cannot capitalize on the increased depths of cut observed in traditional stability lobe diagrams at higher spindle speeds; and
- high machinability materials that are able to take advantage of the increased depths of cut at the "best spindle speeds", which occur at rotating frequencies which are substantial integer fractions of the natural frequency that corresponds to the most flexible structural mode of vibration.

Nearly 50 years of experimental and theoretical investigations have yielded a phenomenological understanding of process damping. Pioneering work was completed by Wallace and Andrew [1], Sisson and Kegg [2], Peters et al. [3], and Tlusty [4]. These studies identified process damping as energy dissipation due to interference between the cutting tool relief, or clearance, face and the machined surface during the inherent relative vibration between the tool and workpiece. It was hypothesized that process damping increases at low cutting speeds because the number of undulations on the machined surface between revolutions (turning) or teeth (milling) increases, which also increases the slope of the wavy surface. This leads to increased interference and, consequently, increased energy dissipation.

Follow-on work has included a plowing force model based on interference between the tool's relief face and workpiece surface [5], application of the plowing force model to milling [6–9], a mechanistic description of the shearing and plowing force contributions to process damping [10], and a first-order Fourier transform representation of the tool-workpiece interference [11,12]. In [13,14], a numerical simulation of a nonlinear process damping stability model was presented, while [15] provided an experimental investigation of a nonlinear process damping model. Experimental identifications of a process damping model were presented in [16,17]. This study builds on the analyses presented in [18–20].

In this paper, an analytical stability analysis is presented that enables multiple degree of freedom (DOF) structural dynamics to be considered, while describing the process damping force in the surface normal direction as a function of the depth of cut, the cutting speed, the tool velocity, and a single empirical coefficient. Because the process damping force is based on the surface normal velocity, which, in general, includes contributions from both orthogonal dynamics directions, a coupled dynamic system is obtained. The analytical solution for turning is presented in the following

* Corresponding author. Tel.: +1 17046875086.
E-mail address: tony.schmitz@uncc.edu (T.L. Schmitz).

http://dx.doi.org/10.1016/j.precisioneng.2016.03.017
0141-6359/

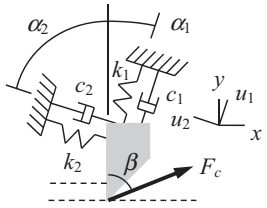

Fig. 1. Turning model with a single DOF in two orthogonal directions.

sections. Validation of the algorithm using time domain simulation and experiments is provided.

2. Stability algorithm

2.1. Single DOF in two directions

The turning model with a single DOF in two orthogonal directions is depicted in Fig. 1. The two mode directions, u_1 and u_2, are oriented at the angles α_1 and α_2, respectively, relative to the surface normal direction, y. The cutting force, F_c, is oriented at the force angle β. The variable component of the cutting force is described by Eq. (1), where K_s is the specific cutting force coefficient, b is the commanded chip width, Y_0 is the vibration amplitude in the y direction from the previous revolution, and Y is the current vibration amplitude. The difference between Y_0 and Y identifies the variable chip thickness due to the vibration from one revolution to the next and provides the basis for regenerative chatter. The mean component of the cutting force is excluded because it does not influence stability for the linear analysis presented here.

$$F_c = K_s b(Y_0 - Y) \tag{1}$$

The assumption for Eq. (1) is that there is no phase shift between the variable force and the chip thickness. This is indicated by the real values of b and K_s. However, it has been shown that a phase shift can occur at low cutting speeds. This phenomenon is captured by the inclusion of the process damping force, F_d, defined in Eq. (2) [17], where C is the process damping coefficient, V is the cutting speed, and $\dot{y}$ is the tool velocity in the y direction. The process damping force is oriented in the y direction and opposes the cutting force (as projected in the y direction). In other words, it is a viscous damping force. Therefore, the process damping force is used to modify the structural damping and obtain an analytical stability solution.

$$F_d = -C\frac{b}{V}\dot{y} \tag{2}$$

To proceed with the solution, the cutting and process damping forces are projected into the u_1 and u_2 directions as shown in Eqs. (3) and (4), where F_{c_1} and F_{c_2} are the cutting force components in the u_1 and u_2 directions.

$$F_{u_1} = F_c\cos(\beta-\alpha_1) - C\frac{b}{V}\dot{y}\cos(\alpha_1) = F_{c_1} - C\frac{b}{V}\dot{y}\cos(\alpha_1) \tag{3}$$

$$F_{u_2} = F_c\cos(\beta+\alpha_2) - C\frac{b}{V}\dot{y}\cos(\alpha_2) = F_{c_2} - C\frac{b}{V}\dot{y}\cos(\alpha_2) \tag{4}$$

The time domain equations of motion for the two directions are provided in Eqs. (5) and (6), where m_i, c_i, and k_i, $i = 1, 2$, are the mass, viscous damping coefficient, and stiffness for the single DOF structural dynamics. In these equations, one overdot indicates one time derivative (velocity) and two overdots indicate two time derivatives (acceleration).

$$m_1\ddot{u}_1 + c_1\dot{u}_1 + k_1u_1 = F_{c_1} - C\frac{b}{V}\dot{y}\cos(\alpha_1) \tag{5}$$

$$m_2\ddot{u}_2 + c_2\dot{u}_2 + k_2u_2 = F_{c_2} - C\frac{b}{V}\dot{y}\cos(\alpha_2) \tag{6}$$

The y direction velocity can be written as a function of the velocities in the u_1 and u_2 directions as shown in Eq. (7). Substitution of Eq. (7) into Eqs. (5) and (6) yields Eqs. (8) and (9). Even though the structural dynamics are uncoupled (orthogonal), the equations of motion for the two directions are now coupled through the $\dot{u}_1$ and $\dot{u}_2$ velocity terms.

$$\dot{y} = \dot{u}_1\cos(\alpha_1) + \dot{u}_2\cos(\alpha_2) \tag{7}$$

$$m_1\ddot{u}_1 + c_1\dot{u}_1 + k_1u_1 = F_{c_1} - C\frac{b}{V}(\dot{u}_1\cos(\alpha_1) + \dot{u}_2\cos(\alpha_2))\cos(\alpha_1) \tag{8}$$

$$m_2\ddot{u}_2 + c_2\dot{u}_2 + k_2u_2 = F_{c_2} - C\frac{b}{V}(\dot{u}_1\cos(\alpha_1) + \dot{u}_2\cos(\alpha_2))\cos(\alpha_2) \tag{9}$$

By assuming a solution of the form $u_1(t) = U_1e^{i\omega t}$ for harmonic motion, Eqs. (8) and (9) can be rewritten in the frequency domain (ω is frequency). The results are provided in Eqs. (10) and (11), where the U_1 and U_2 terms have been grouped on the left hand side in both equations and the $e^{i\omega t}$ term has been dropped from both sides in each case.

$$\left(-m_1\omega^2 + i\omega\left(c_1 + C\frac{b}{V}(\cos(\alpha_1))^2\right) + k_1\right)U_1 + i\omega\left(C\frac{b}{V}\cos(\alpha_1)\cos(\alpha_2)\right)U_2 = F_{c_1} \tag{10}$$

$$\left(-m_2\omega^2 + i\omega\left(c_2 + C\frac{b}{V}(\cos(\alpha_2))^2\right) + k_2\right)U_2 + i\omega\left(C\frac{b}{V}\cos(\alpha_1)\cos(\alpha_2)\right)U_1 = F_{c_2} \tag{11}$$

These equations are arranged in matrix form as shown in Eq. (12), where:

- $a_{11} = \left(-m_1\omega^2 + i\omega\left(c_1 + C\frac{b}{V}(\cos(\alpha_1))^2\right) + k_1\right)$
- $a_{12} = i\omega\left(C\frac{b}{V}\cos(\alpha_1)\cos(\alpha_2)\right)$
- $a_{21} = a_{12}$
- $a_{22} = \left(-m_2\omega^2 + i\omega\left(c_2 + C\frac{b}{V}(\cos(\alpha_2))^2\right) + k_2\right)$.

$$\begin{bmatrix} a_{11} & a_{12} \\ a_{21} & a_{22} \end{bmatrix}\begin{bmatrix} U_1 \\ U_2 \end{bmatrix} = \begin{bmatrix} F_{c_1} \\ F_{c_2} \end{bmatrix} \tag{12}$$

Using complex matrix inversion on a frequency-by-frequency basis, the direct and cross frequency response functions (FRFs) for the coupled dynamic system are obtained as shown in Eq. (13). The direct FRFs are located in the on-diagonal positions and the cross FRFs are located in the off-diagonal positions; the cross FRFs are equal because the inverted matrix is symmetric.

$$\begin{bmatrix} U_1 \\ U_2 \end{bmatrix} = \begin{bmatrix} a_{11} & a_{12} \\ a_{21} & a_{22} \end{bmatrix}^{-1}\begin{bmatrix} F_{c_1} \\ F_{c_2} \end{bmatrix} = \begin{bmatrix} \frac{U_1}{F_{c_1}} & \frac{U_1}{F_{c_2}} \\ \frac{U_2}{F_{c_1}} & \frac{U_2}{F_{c_2}} \end{bmatrix}\begin{bmatrix} F_{c_1} \\ F_{c_2} \end{bmatrix} \tag{13}$$

Tlusty [21] provided a frequency domain stability solution for regenerative chatter in turning, which defines the limiting stable chip width, b_{lim}, using Eq. (14), where $Re(G_{or})$ is the negative portion of the real part of the oriented FRF, G_{or}. This oriented FRF represents the projection of the cutting force into the mode direction and then the projection of this result in the surface normal direction.

$$b_{\lim} = \frac{-1}{2K_sRe(G_{or})} \tag{14}$$

To relate the frequency-dependent b_{lim} vector to the spindle speed, Ω, Eq. (15) is applied to determine the relationship between and the valid chatter frequencies, f_c (i.e., those frequencies where $Re(G_{or})$ is negative). In this equation, $N = 0, 1, 2, \ldots$ is the integer number of waves per revolution (i.e., the lobe number) and

Please cite this article in press as: Tyler CT, et al. A coupled dynamics, multiple degree of freedom process damping model, Part 1: Turning. Precis Eng (2016), http://dx.doi.org/10.1016/j.precisioneng.2016.03.017